Sādhanā (2020) 45:253
https://doi.org/10.1007/s12046-020-01493-0

Experimental investigation of magnetic-field-assisted electric discharge machining by silicon-based dielectric of Inconel 706 superalloy

SUSHIL KUMAR*, MUDIMALLANA GOUD and NARENDRA MOHAN SURI

Department of Production and Industrial Engineering, Punjab Engineering College (Deemed to be University), Chandigarh 160012, India
e-mail: sushil09988031869@gmail.com; mudigoud@gmail.com; nmsuri65@yahoo.com

MS received 5 March 2020; revised 1 August 2020; accepted 29 August 2020

Abstract. Inconel 706 is a nickel–iron-based superalloy having higher mechanical strength along with easiness of fabrication, which makes it suitable for gas turbine disk applications. The current study investigates the hybrid magnetic-field-assisted powder mixed electric discharge machining (MFAPMEDM) process to improve performance in machining Inconel 706. For conducting experiments, an in-house set-up was designed and fabricated. Experiments were conducted according to the Taguchi L9 OA and ANOVA to examine the effect of the peak current (I_p) and pulse duration (P-on/P-off) on the material removal rate (MRR) and surface roughness (R_a) of the machined samples. The quality of the machined surface is assessed using a field emission scanning electron microscope (FESEM), which has revealed the presence of micro-holes, melted debris and micro-globules on the machined specimen surface. The R_a is significantly affected by I_p (49.63%) and P-off (37.12%). Further, I_p has more than 78% contribution to the MRR. Furthermore, a mathematical model has been established to develop the relation between input and output factors.

Keywords. EDM; Inconel 706; silicon carbide; magnetic field; FESEM.

1. Introduction

Inconel 706 is an advanced superalloy that possesses higher strength along with ease of fabricability [1]. Inconel 706 can be shaped with large size diameter, which makes it convenient for making turbine disks owing to its outstanding chemical stability and being less susceptible to segregation phenomenon [2, 3]. Improved gas turbine engines need higher firing temperature and compression ratio, which makes it essential to employ Inconel 706 for the rotors [4]. The high fatigue strength of nickel-based superalloys even at increased service temperature is a perfect choice for numerous industries, including the aerospace sector. Nevertheless, it is difficult to machine these superalloys [5]. Generally, the machining through the conventional processes of these superalloys offers poor machining efficiency, minimum dimensional characteristics and poor surface attribute of the specimens produced. These types of challenges are often because of the phenomenon of work-hardening, abrasive nature and lower thermal conductivity of these superalloys [6, 7]. Therefore, to resolve these problems, the non-traditional machining processes such as abrasive water jet machining (AWJM), electrochemical machining (ECM), wire electrical discharge machining (WEDM) and laser beam machining (LBM) are successfully employed for machining of these superalloys [8–11].

Out of several non-conventional methods, electric discharge machining (EDM) is popular, specifically for die and mould making industries [12]. EDM is a commonly utilized non-traditional machining method of processing any electrically conductive workpiece into complicated and intrinsic shapes [13]. However, there are some challenges related to the EDM concerning lesser material removal rate (MRR) and poor machined surface quality of the parts produced [14].

For surmounting these drawbacks, certain modifications have been made by mixing powders with dielectric as it enables attaining higher MRR and low R_a. The alteration in plasma channel takes place through mixing of powder particles with the dielectric, which extends and broadens the plasma channel. Multiple sparks among the powder particles help in distributing the discharge energy over a large area. It causes large and shallow craters on the surface of the workpiece. The MRR increases with increase in number of wide craters [15]. Furthermore, the molten material is not deeply forced by the plasma and the gas bubble. The gas trapped in the craters decreases depending

*For correspondence
Published online: 07 October 2020

on these conditions, which makes the surface uniform, less concave and even [16]. Nevertheless the addition of powder is regulated through unwanted arcing, as arc causes severe damage to the surface, thus reducing MRR. Further, the powder gives rise to a number of arcs instead of sparks [17]. The addition of carbon nanotubes in the dielectric affects MRR as well as the surface cracks on machined specimens [18]. In another investigation, researchers concluded that adding aluminium oxide (Al_2O_3) nano-powders into the dielectric media causes increase in MRR and decrease in R_a compared with the traditional EDM in machining Inconel 825 material with copper as a tool electrode [19]. Researchers have carried out EDM experiments by adding graphite, Si and Al powders to the dielectric media and observed that compared with the traditional EDM, the addition of powder causes augmentation of MRR, development of hardened layer underneath the machined surface, reducing surface roughness, and minimal surface cracks [17]. In comparison with the traditional EDM process the topographical aspects of machined Inconel 718 were examined after adding SiC powder into dielectric media, and it caused enhanced MRR, decreased R_a, reduced TWR and reduced surface crack density (SCD) [20].

Another modification is done by producing magnetic field environment to enhance the material removal, and R_a is reduced in traditional EDM. The magnetic field together with electric field generates Lorentz force and modifies the path of electrolytic ions. The procedure effectively ejects machining debris and clears the gap, thereby augmenting MRR [21]. The MRR in magnetic field environment is augmented by changing the molten debris distance further from the crater, escalating amount of erosion and sustaining steady discharge waves through the cleaning of gap [22] both for traditional EDM and dry EDM [23]. Lin and Lee [21] stated that magnetic force can enhance MRR by three times and can decrease R_a to $1/3^{rd}$. Existence or influence of the magnetic field around the machining area improves the expulsion of debris, and thereby the overall effectiveness of the process [24]. Researchers observed the influence of magnetic field on MRR and R_a [25, 26]. The uniqueness of this process in terms of MRR and TWR is related to the effect with the chemistry of the magnetic field environment on the EDM process as is also evident in the outcomes [27]. The possibility and features of this process indicate that the Lorentz force adds up a thrust force on the crater at the time of the spark discharge having an external magnetic field [28].

Many researchers have reported about the enhancement of process in EDM using the combination of powder-mixed and magnetic-field-assisted EDM. Researchers demonstrated the alteration of surface using Al–55% SiC MMC by silicon carbide mixed magnetic field-assisted EDM [29]. Current acts as a significant parameter at the time of machining different grades of steel through use of graphite, tungsten and titanium powder suspended in the EDM oil in conjunction with the magnetic field [30]. The impact of machining parameters on the microstructure was scrutinized, and the augmentation of micro-hardness was perceived while machining various grades of steel with the use of titanium and tungsten powder considering the effect of magnetic field [31].

Limited research has been done in the field of hybrid machining (by MFAPMEDM) of Inconel 706 superalloy. Therefore, there are wide range of possibilities to analyse the machining performance and to optimize the machining parameters during the machining of Inconel 706. In this study, an innovative set-up (process) was developed and employed to study the influence of critical input parameters of the MFAPMEDM process for improving the productivity besides better quality of the surface. Further, electron microscopy was used to analyse the machined surface topography.

2. Materials selection and methodology

2.1 *Materials*

Inconel 706 was chosen as a base material, as it is considered as a preferable superalloy for turbine disk application over Inconel 718 because of the lesser percentage of alloying elements and ease of fabrication [32]. Table 1 shows the chemical composition of Inconel 706. The material was procured from ''Antriksh Metal Corporation', India' in the form of a billet of dimensions 300 mm × 200 mm × 5 mm. Specimens of size 25 mm × 25 mm × 5 mm were prepared for machining experiments. The mechanical and physical properties of the base material are tabulated in Table 2.

2.2 *Experimental details*

Investigational work was done on EDM (Model: ELEKTRAPULS PS 35 from Electronica Machine Tools, Pune, India), wherein a special in-house set-up was fabricated with a pump attached for homogeneous mixing of SiC particles along with flushing of these particles. Besides pump, a stirring arrangement was attached for continuous stirring and mixing of SiC abrasive particles of 650 mesh size in dielectric medium of commercial-grade EDM oil with the concentration of 10 gm/l to avoid settling down. The effect of the turbulence generated during the rotation of the dielectric fluid was neglected. Figure 1(a) shows the EDM machine employed for conducting experiments. The experiments were performed with copper as tool material and the SiC-based dielectric medium was used for optimization of input process parameters. SiC-based dielectric was prepared and utilized for conducting experiments with the powder concentration of 10 gm/l. Figure 1(b) shows that the permanent magnets set-up arrangement is planned

Table 1. Inconel 706 chemical composition [32].

Alloy (%)		Ni+Co	Cr	Nb+Ta	Fe	Co	C	Ti	Si	Cu	S	Mn	P	Al
Inconel 706 alloy	Min.	39	14.5	2.5	Bal.	–	–	1.5	–	–	–	–	–	–
	Max.	44	17.5	3.3		1	0.06	2	0.35	0.3	0.02	0.35	0.02	0.4

Table 2. Properties of Inconel 706 [32].

Properties	Specification
Melting temperature range	1334–1371 °C
Density	8.05 g/cm^3
Modulus of elasticity	210 kN/mm^2
Thermal conductivity	12.5 W/mK
Yield strength	993 MPa
Tensile strength	1282 MPa
Elongation	19%

near the workpiece and tool by maintaining the separation of 40 mm among the magnetic poles (i.e. facing front) on the opposing sides. A couple of square-shaped permanent magnets (0.33 T each) of measurements 50 mm × 50 mm × 15 mm of N-50 grade were engaged to provide a magnetic field near the machining area. Figure 1(c) shows a schematic of the arranged set-up.

2.3 *Input parameters*

The input control variables selected were I_p, P-off and P-on during machining of the Inconel 706 in the magnetic field of 0.33 T intensity. The machining parameters were selected by keeping machining constraints in mind. The prominent process parameters with the help of initial trial experiments were recognized. The input variables (Table 3) varied at three different levels in the magnetic field, which were carefully chosen to conduct the MFAPMEDM process using positive polarity. For a complete evaluation of process parameters, a total of 27 experiments were performed. However, taking the complexity and cost factor into consideration, Taguchi L9 OA was selected. This array helps in reducing the exhaust experimentations without altering the significance of experimentations. Various trials were conducted as per L9 OA (Table 4).

2.4 *Response parameters*

The outcome of controlled input parameters was studied on MRR and R_a in machining of Inconel 706. A magnetic field of 0.33 T intensity was established near the spark, along these lines, thus disturbing the standard flow of current during the MFAPMEDM process. The MRR has been calculated using the weight reduction technique and determined as given in equation (1):

$$\text{MRR} = \frac{W_b - W_a}{\rho t} \tag{1}$$

where W_b is weight of the sample before machining (g), W_a is weight of the sample after machining (g), ρ is density of the workpiece material (g/mm^3) and t is the machining time (s).

All machined samples were weighed up using a Denver SI 234 digital weighing machine (accuracy of 0.01 mg). The moisture content was removed with the use of a hot air blower for drying before weighing. The machining duration was calculated using a digital stopwatch. For R_a, the machined specimens were examined using a 'Mitutoyo-Surftest SJ-400' surface roughness tester [33]. The R_a of all the samples was measured diametrically at three different positions within the machined region, and the mean was reported. The Japanese made Hitachi SU 8010 Series, FESEM (field emission scanning electron microscope) facility was used to analyse the surface topography of machined samples.

3. Results and discussion

The machined surface topography has been explained through FESEM images in the MFAPMEDM process. The settings of the controlled input parameters are designed and enhanced according to the L9 OA and output variables, and the results of response parameters for each machined specimen with corresponding *S/N* ratio values as well as in the presence of 0.33 T intensity magnetic field are recorded in Table 4. A relative assessment of MRR and R_a for machined samples affected by the magnetic field during machining with copper as a tool electrode in SiC-based dielectric medium is shown in Table 5. For analysing the response outcomes, Minitab (version 18.0) package was used.

3.1 *Influence of input parameters on MRR*

Figure 2 shows the main effects plot for MRR. From Figure 2 and Table 5, it can be observed that I_p plays a significant role in machining followed by P-on and P-off for MRR. With increase in the I_p the MRR increases because

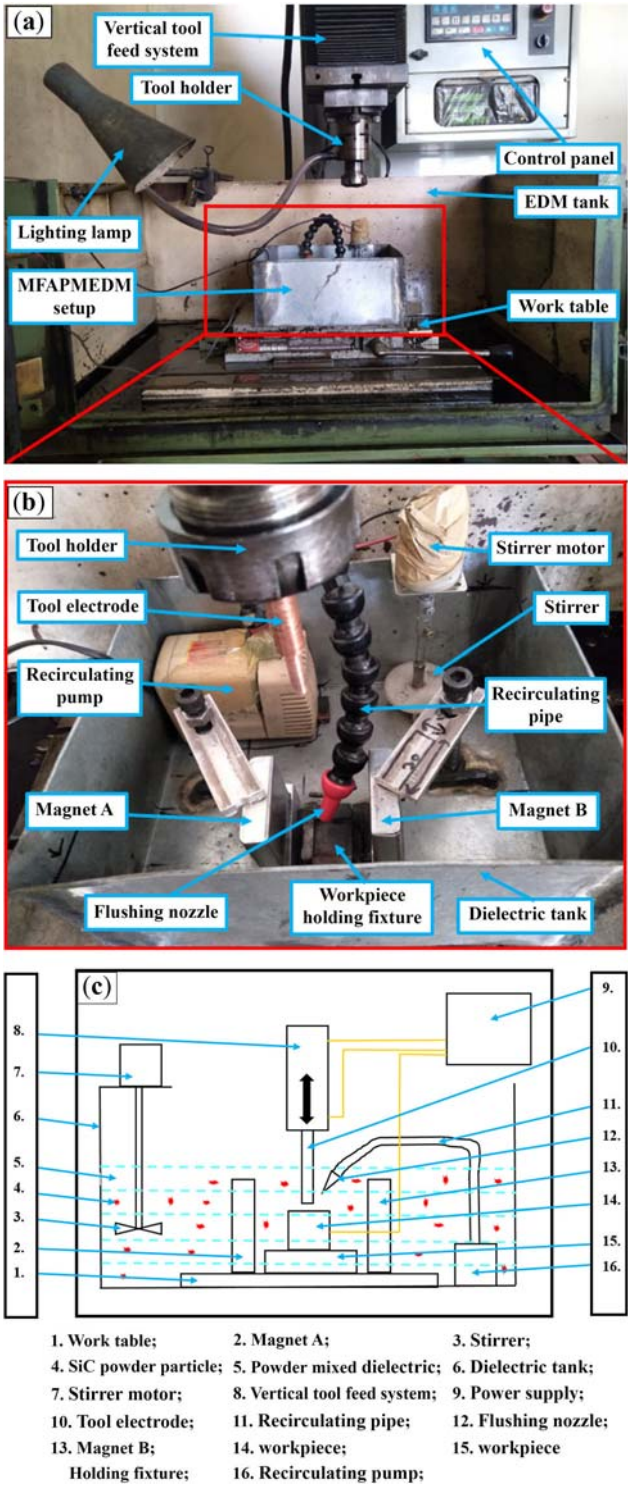

Figure 1. (a) ELEKTRAPULS CNC EDM machine, (b) apparatus for MFAPMEDM set-up and (c) schematic for the set-up.

the escalation of I_p leads to an increase in energy per pulse, which further results in the rise of temperature, and it causes quick melting of work surface at the sparking area, which accounts for the more quantity of material removal from the base material. The intensity of the spark increases at higher P-on, which ensues the removal of relatively more volume of material from the machining area, thus resulting in higher MRR. Furthermore, MRR decreases with increase in P-off because the number of sparks reduces in a given time, thereby reducing the crater size made on the specimen surface, which tends to lesser MRR. From the *S*/*N* plot, the optimal parametric set for MRR is A3B3C1.

Table 3. Input process parameters.

Parameter	Peak current	Pulse-on time	Pulse-off time
(Units/symbols)	I_p (A)	P-on (μs)	P-off (μs)
Level 1	5	10	10
Level 2	10	30	20
Level 3	15	50	30

3.2 *Influence of input parameters on R_a*

Figure 3 shows the main effects plot for R_a. From Figure 3 and Table 5, it can be observed that I_p plays a significant role in machining followed by P-off and P-on for R_a. With the increase in I_p the spark intensity per pulse increases, thus resulting in a larger crater depth formation on the work surface, thereby resulting in the increase of R_a. Furthermore, at higher P-off, the increase in the cooling and flushing duration tends to spill out somewhat extra quantity of molten material, resulting in the decrease of R_a. It has been detected that R_a increases as P-on increases because the spark intensity increase at higher P-on, thus making a larger and deeper crater into the workpiece material, which in turn leads to higher R_a. To reduce the R_a, P-on and I_p should be less with higher pulse-off interval. From the *S*/*N* plot, the optimal parametric set for R_a is A1B1C3.

3.3 *Surface topography analysis*

The influence of input parameters on the machined surface was examined to analyse the surface topography using the FESEM micrographs (Figure 4). The micrographs show the presence of micro-holes, micro-globules and melted debris on the machined surface. It is a known fact that the formation of craters and micro-holes is the result of high thermal energy released from a spark, which increases the material temperature within the range of ∼ 10,000 °C, which is sufficient for its melting and vaporization. However all the molten material cannot be splashed from the machining area owing to inadequate exploding pressure, thereby resulting in the trapping of the gas bubbles inside the molten material and its solidification on the surface itself.

Higher number of micro-holes, micro-globules and molten debris were formed on the specimen's surface with

Table 4. L9 Investigational design and responses.

	Process parameters			Responses			
Sl. no.	I_p (A)	P-on (μs)	P-off (μs)	MRR (mm^3/min)	*S/N* ratio (dB)	R_a (μm)	*S/N* ratio (dB)
1	5	10	10	2.424	7.6921	0.014	37.0774
2	5	30	20	1.863	5.4052	0.027	31.3727
3	5	50	30	1.718	4.7010	0.0175	35.1392
4	10	10	20	5.290	14.4691	0.0715	22.9139
5	10	30	30	7.986	18.0466	0.0325	29.7623
6	10	50	10	14.476	23.2130	0.198	14.0667
7	15	10	30	18.915	25.5361	0.07	23.0980
8	15	30	10	21.175	26.5165	0.27375	11.2529
9	15	50	20	43.500	32.7698	0.144	16.8328

Table 5. ANOVA table for MRR and R_a.

			Analysis MRR				Analysis R_a			
Sl. no.	Control factors	DF	Adj SS	Adj MS	*F*-value	%age cont.	Adj SS	Adj MS	*F*-value	%age cont.
1	I_p	2	1067.79	533.89	9.07	78.25	0.030895	0.015447	6.15	49.63
2	P-on	2	214.95	107.48	1.83	15.78	0.008211	0.004106	1.64	13.23
3	P-off	2	81.46	40.73	0.69	5.95	0.023106	0.011553	4.60	37.12
4	Error	2	117.77	58.89			0.005020	0.002510		
5	Total	8	1481.97				0.067231			

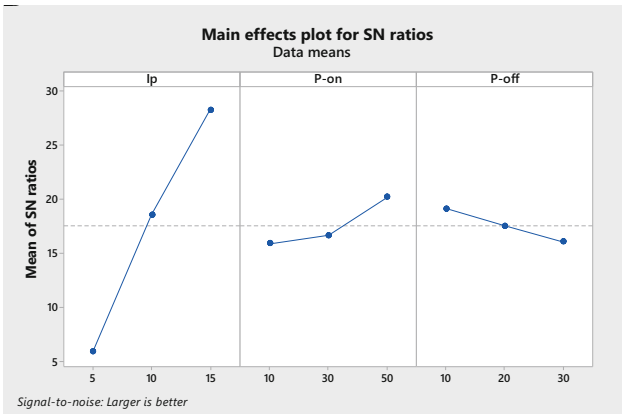

Figure 2. Main effects plot for MRR.

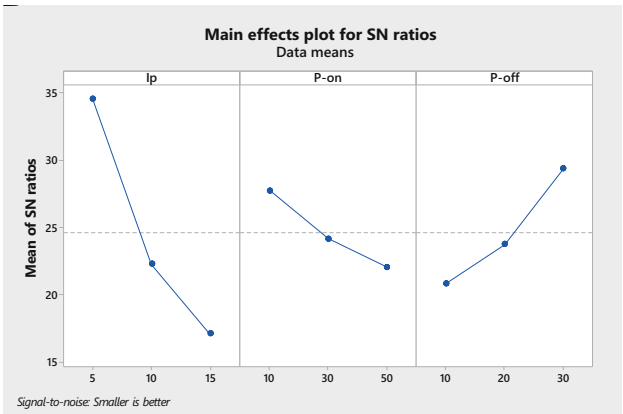

Figure 3. Main effects plot for R_a.

increase in the value of I_p. This is because more thermal energy is released from the discharge, which helps in the formation of large size craters on the surface (Figure 4(b); Experiment No. 9). It further leads to the deterioration of the surface quality of the samples. On the contrary, the lower I_p produced surfaces with smoother quality along with reduced melted debris and micro-holes (Figure 4(a); Experiment No. 2). A higher magnification FESEM micrograph of the machined sample (Figure 4(c); Experiment No. 5) indicates that a few micro-holes and partially melted debris are present upon machining at a higher P-off. It was explained that the increase in P-off resulted in the decrease of the spark intensity and augmented the cooling time. Subsequently the formation of micro-globules and micro-holes was reduced, which enhanced the quality of the specimen's surface.

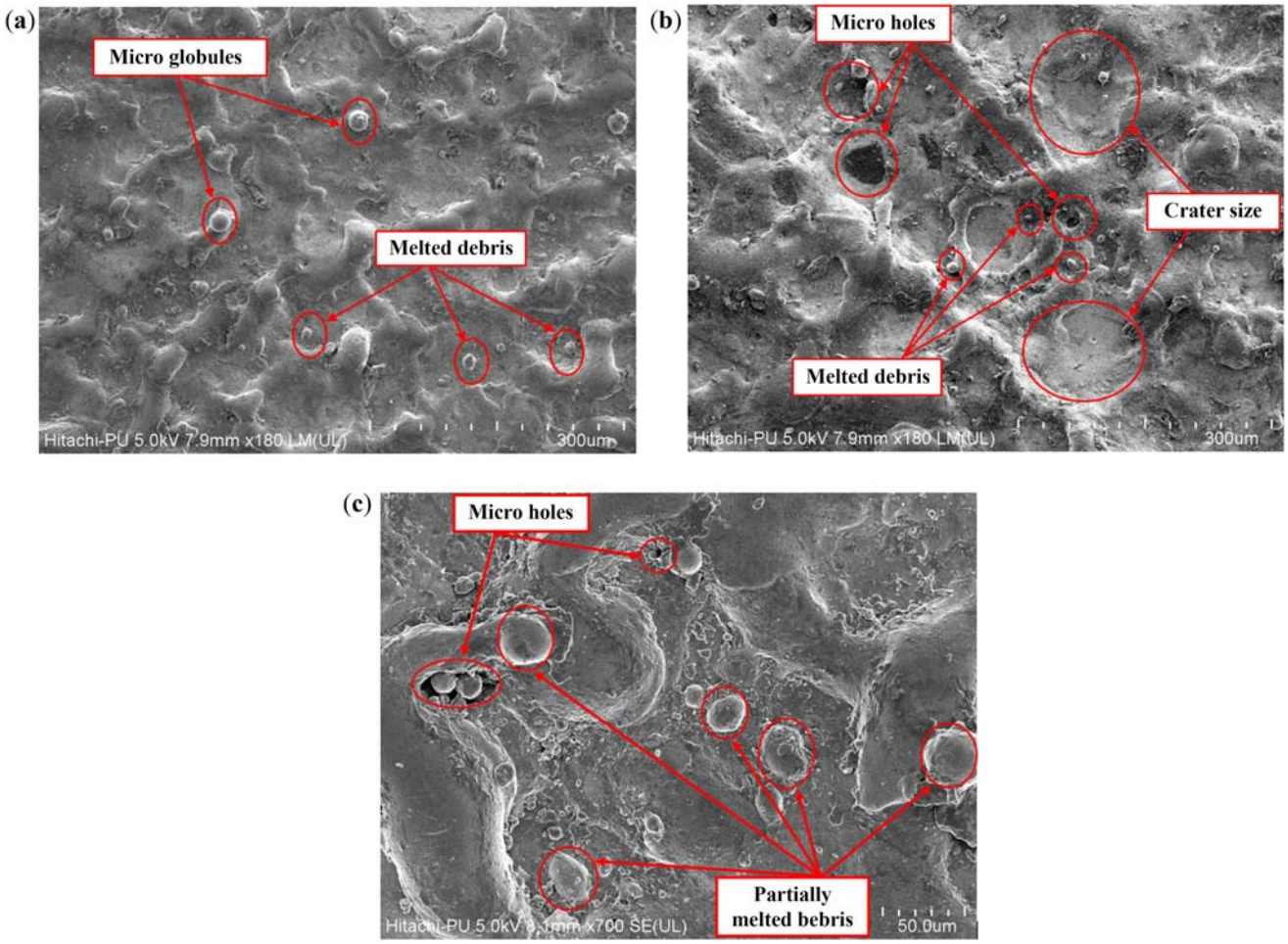

Figure 4. FESEM micrographs for the surface topography analysis of machined surface: (a) Experiment No. 2, (b) Experiment No. 9 and (c) Experiment No. 5.

3.4 *Mathematical modelling*

A multiple regression model was prepared to develop the relationship between the control input factors regarding the output characteristics by fitting the linear equation for the recorded experimental values. The interaction effect of input factors was not measured because of the chosen L9 OA. The fixed parameters, such as anode, cathode and dielectric concentration were taken into consideration as limitations while preparing this model. Equations (2) and (3) can be employed to machine Inconel 706 by the MFAPMEDM process at various working parameters keeping the other constant factors in mind. The following mathematical expressions are for MRR and R_a, respectively, developed using Minitab (version 18.0):

The mathematical model for MRR (mm^3/min) is

$$\begin{aligned} &\text{MRR} = -17.9 + 2.586\left(I_p\right) + 0.276(\text{Pon}) - 0.158(\text{Poff}),\\ &R^2(\text{MRR}) = 81.00\%, \end{aligned} \tag{2}$$

The mathematical model for R_a (μm) is

$$\begin{aligned} &R_a = 0.0221 + 0.01431\left(I_p\right) + 0.001700(\text{Pon}) - 0.00610(\text{Poff}),\\ &R^2(R_a) = 89.16\%. \end{aligned} \tag{3}$$

4. Conclusions

In this study, the hybrid MFAPMEDM process is utilized to machine Inconel 706 superalloy. A test examination is conducted to examine the impact of I_p, P-on and P-off duration. The subsequent observations are drawn after the investigational study on the MRR and R_a features for machining of Inconel 706.

- The in-house MFAPMEDM set-up can effectively machine the Inconel 706 material.
- Based on an *S/N* ratio, higher I_p and higher P-on are suggested for higher MRR since the ANOVA result reveals that they contribute 78.25% and 15.78%, respectively.

- For minimum R_a, I_p and P-off are the most important parameters. The ANOVA results reveal that I_p and P-off contribute 49.63% and 37.12%, respectively.
- Surface topography has shown that micro-holes and melted debris are more prominent in Experiment No. 9 because of the higher I_p and higher P-on and therefore offers a rougher surface on the machined component. The presence of micro-holes and micro-globules decreases notably at lower values of I_p.
- Surface topography also shows the curved shape profile and the minimum R_a of the machined specimen is witnessed in Experiment No. 2 owing to lower value of I_p and increased P-off, thus offering a fine and smoother machined surface of the specimen through proper flushing of the melted debris.

Nomenclature

MFAPMEDM	Magnetic-field-assisted powder mixed electrical discharge machining
EDM	Electrical discharge machining
dB	Decibels
T	Tesla
I_p	Peak current
P-off	Pulse-off time
P-on	Pulse-on time
R_a	Surface roughness
MRR	Material removal rate
SiC	Silicon carbide
TWR	Tool wear rate
FESEM	Field emission scanning electron microscope
S/*N* ratio	Signal to noise ratio
OA	Orthogonal array
DF	Degrees of freedom
Adj MS	Adjusted mean square
Adj SS	Adjusted sums of squares
ANOVA	Analysis of variance

References

[1] Sharma P, Chakradhar D and Narendranath S 2015 Evaluation of WEDM performance characteristics of Inconel 706 for turbine disk application. *Mater. Des.* 88: 558–566

[2] Sharma P, Chakradhar D and Narendranath S 2016 Effect of wire material on productivity and surface integrity of WEDM processed Inconel 706 for aircraft application. *J. Mater. Eng. Perform.* 25(9): 3672–3681

[3] Sharma P, Chakradhar D and Narendanath S 2016 Effect of wire diameter on surface integrity of wire electrical discharge machined Inconel 706 for gas turbine application. *J. Manuf. Process.* 24: 170–178

[4] Muktinutalapati N R 2011 *Materials for gas turbines – an overview*. INTECH Open Access Publisher

[5] Naskar A, Singh B B, Choudhary A and Paul S 2018 Effect of different grinding fluids applied in minimum quantity cooling-lubrication mode on surface integrity in cBN grinding of Inconel 718. *J. Manuf. Process.* 36: 44–50

[6] Sinha M K, Madarkar R, Ghosh S and Paruchuri V R 2018 Some investigations in grindability improvement of Inconel 718 under ecological grinding. *Proc. Inst. Mech. Eng. B: J. Eng. Manuf.* https://doi.org/10.1177/0954405417752513

[7] Sinha M K, Ghosh S and Paruchuri V R 2017 Modelling of specific grinding energy for Inconel 718 superalloy. *Proc. Inst. Mech. Eng. B: J. Eng. Manuf.* https://doi.org/10.1177/0954405417741513

[8] Singh J and Jain S C 1995 Mechanical issues in laser and abrasive water jet cutting. *J. Min. Met. Mater. Soc.* 47(1): 28–30

[9] El-Hofy H 2005 *Advanced machining processes: non-traditional and hybrid machining processes*. McGraw Hill Professional

[10] Sharma P, Chakradhar D and Narendranath S 2017 Analysis and optimization of WEDM performance characteristics of Inconel 706 for aerospace application. *Silicon*, https://doi.org/10.1007/s12633-017-9549-6

[11] Zhong M, Sun H, Liu W, Zhu X and He J 2005 Boundary liquation and interface cracking characterization in laser deposition of Inconel 738 on directionally solidified Ni-based superalloy. *Scr. Mater.* 53(2): 159–164

[12] Jadam T, Sahu S K, Datta S and Masanta M 2020 Powder-mixed electro-discharge machining performance of Inconel 718: effect of concentration of multi-walled carbon nanotube added to the dielectric media. *Sådhanå* 45: 135, https://doi.org/10.1007/s12046-020-01378-2

[13] Talla G, Gangopadhyay S and Biswas C K 2017 Influence of graphite powder mixed EDM on the surface integrity characteristics of Inconel 625. *Particul. Sci. Technol.* 35(2): 219–226

[14] Talla G and Gangopadhyay S 2016 Effect of impregnated powder materials on surface integrity aspects of Inconel 625 during electrical discharge machining. *Proc. Inst. Mech. Eng. B: J. Eng. Manuf.* https://doi.org/10.1177/0954405416666904

[15] Fong T Y and Chen F C 2005 Investigation into some surface characteristics of electrical discharge machined SKD-11 using powder-suspension dielectric oil. *J. Mater. Process. Technol.* 170: 385–391

[16] Tzeng Y F and Lee C Y 2001 Effects of powder characteristics on electrodischarge machining efficiency. *Int. J. Adv. Manuf. Technol.* 17: 586–592

[17] Talla G, Gangopadhyay S and Biswas C K 2016 Effect of powder-suspended dielectric on the EDM characteristics of Inconel 625. *J. Mater. Eng. Perform.* 25(2): 704–717

[18] Shabgard M and Khosrozadeh B 2017 Investigation of carbon nanotube added dielectric on the surface characteristics and machining performance of Ti–6Al–4V alloy in EDM process. *J. Manuf. Proc.* 25: 212–219

[19] Kumar A, Mandal A, Dixit A R, Das A K, Kumar S and Ranjan R 2018 Comparison in the performance of EDM and NPMEDM using Al_2O_3 nanopowder as an impurity in DI water dielectric. *Int. J. Adv. Manuf. Technol.* https://doi.org/10.1007/s00170-018-3126-z

[20] Sahu S K, Jadam T, Datta S and Nandi G 2018 Effect of using SiC powder-added dielectric media during electro-discharge machining of Inconel 718 superalloys. *J. Braz. Soc. Mech. Sci. Eng*. 40: 330 https://doi.org/10.1007/s40430-018-1257-7

[21] Lin Y C and Lee H S 2008 Machining characteristics of magnetic force-assisted EDM. *Int. J. Mach. Tool Manuf.* 48: 1179–1186

[22] Heinz K, Kapoor S G, Devor R E and Surla V 2011An investigation of magnetic-field-assisted material removal in micro-EDM for nonmagnetic materials. *J. Manuf. Sci. Eng*. 133(021002): 9

[23] Joshi S, Govindan P, Malshe A and Rajurkar K 2011 Experimental characterization of dry EDM performed in a pulsating magnetic field. *CIRP Ann. Manuf. Technol.* 60: 239–242

[24] Yeo S H, Murali M and Cheah H T 2004 Magnetic field assisted microelectro-discharge machining. *J. Micromech. Microeng.* 14: 1526–1529

[25] Rattan N and Mulik R S 2017 Experimental investigations and multi-response optimization of silicon dioxide (quartz) machining in magnetic field assisted TW-ECSM process. *Silicon* 9: 663–673

[26] Yamaguchi H and Shinmura T 2004 Internal finishing process for alumina ceramic components by a magnetic field assisted finishing process. *Prec. Eng.* 28: 135–142

[27] Chattopadhyay K D, Satsangi P S, Verma S and Sharma P C 2008 Analysis of rotary electrical discharge machining characteristics in reversal magnetic field for copper-en8 steel system. *Int. J. Adv. Manuf. Technol.* 38: 925–937

[28] Bains P S, Sidhu S S and Payal H S 2016 Study of magnetic field assisted ED machining of metal matrix composites. *Mater. Manuf. Process.* 31(14): 1889–1894

[29] Bains P S, Sidhu S S, Payal H S and Kaur S 2018 Magnetic field influence on surface modifications in powder mixed EDM. *Silicon* https://doi.org/10.1007/s12633-018-9907-z

[30] Bhatt G, Batish A and Bhattacharya A 2015 Experimental investigation of magnetic field assisted powder mixed electric discharge machining. *Particul. Sci. Technol.* 33(3): 246–256

[31] Bhattacharya A, Batish A and Bhatt G 2015 Material transfer mechanism during magnetic field–assisted electric discharge machining of AISI D2, D3 and H13 die steel. *Proc. Inst. Mech. Eng. B: J. Eng. Manuf*. 229(1): 62–74

[32] *Inconel alloy 706*. Technical bulletin, Publication Number SMC-091. Special Metals Corporation, retrieved from: http://www.specialmetals.com/assets/documents/alloys/inconel/inconel-alloy-706.pdf

[33] Kumar M, Vaishya R O, Oza A D and Suri N M 2019 Experimental investigation of wire-electrochemical discharge machining (WECDM) performance characteristics for quartz material. *Silicon* https://doi.org/10.1007/s12633-019-00309-z